ENERGY EFFICIENT ACTIVE CONTROL OF THE FLOW PAST AIRCRAFT WINGS

V. Skarolek and S.J. Karabelas*

Institute of Aerospace Engineering, Faculty of Mechanical Engineering, Brno University of Technology, Technická 2896/2, 616 69 Brno, Czech Republic

Abstract

Numerical simulations of the flow past a NACA 0015 wing with active control have been performed. The Reynolds number of the flow is 2.5 x 10^6. The configuration proposed in this study does not follow the conventional active control methodology past wings. Large blowing surfaces and low jet velocity magnitudes are considered and the energy efficiency of such configuration is examined for a number of variants. One major impact on the flow is the diffusion of the tip vortex core in the trailing edge area, but also farther downstream. Strategies for drag reduction and lift increase of the wing are proposed by varying some of the actuation parameters. The present active flow control could be efficient at all angles of attack, while in the same time could be able to reduce significantly the total drag of the wing, increase the total lift or combine effectively those favorable effects for better flight performance. Maximum drag decrease could exceed 40% of the total drag at low angles of attack, with still positive energy income.

Keywords: active flow control; control surfaces; high Reynolds; wing; blowing; drag reduction

*Corresponding author:
Email-address:stkarabelas@yahoo.gr

1. Introduction

Active flow control studies in industry and literature are oriented mainly towards two main directions: 1. to reduce the induced drag of the aircraft's wings and 2. to diffuse the wake vortex in such a way, that its' decay in atmosphere will be faster (lower level of hazards in air-traffic). In literature, a large amount of relevant studies correlated to the aforementioned fields, could be referenced. One of the first studies, which concerned experimental axial wing-tip blowing, was performed by Dunham (1976). More recently, a numerical study conducted by Lim (1994), revealed that this active flow control in drag reduction terms is completely unsuccessful, although it affects significantly the flow-field downstream of the wing. Dunham (1976) classified also this concept, as an unsuccessful control for faster vortex decay. A second major type of active flow control, which has been implemented for altering the development of the wake-vortex and reducing the induced-drag, is blowing towards the span-wise direction. This concept is based on the thought, that it could be possible by blowing laterally to increase the effective aspect ratio and shift the vortex outboard. Tavella and Roberts (1985) demonstrated this control with high velocity ratio jets. Mineck (1995) performed numerical and experimental investigation of the flow past a wing with active span-wise blowing. After examining multiple configurations, it was concluded that it is possible to reduce the drag of the wing with the implementation of longer jets at the wing-tip area. Nevertheless, the energy consumption was higher from the gained energy from the drag reduction, making this concept ineffective in energy terms. Coimbra and Catalano (2002) performed blowing from the wing tip area towards multiple directions. The aerodynamic performance of the wing is considerably increased in terms of the lift and drag forces. However, based on their referenced momentum coefficients, the demanding energy appears to be many times higher than the benefit. A highlighted experimental study is also that one of Margaris and Gursul (2010), who performed continuous blowing from the tip area towards the vertical and the span-wise direction. Those configurations in some cases diffuse more the main tip vortex in the near downstream area, which seems to be really promising concept for reducing the time separation of aircraft operations in heavy air-traffic conditions. Nevertheless, the active flow control configurations are proved to be again energy inefficient. Another type of active flow control is pulsed blowing. This concept gains more interest, because of the general energy efficiency (piezoelectric membranes) and the still open space for attaining drag reduction and total lift. A detailed study is performed by Heyes and Smith (2004), who imposed cyclic spatial perturbation in the trailing vortex trajectory by using high velocity ratio jets. Increase of the vortex core radius and decrease in the peak tangential velocities are the main findings of this research. Decomposition of the vortex was also observed in the study of Yadlin and Shmilovic (2008). Nevertheless, no concrete results regarding the load terms are quoted.

From the above studies, it becomes evident that the conventional methods of active control do not improve the aerodynamic efficiency of the wing and if they improve it, they are proved to be energy inefficient. In the present research study, a different approach is adopted to reduce the total drag of the wing. The core idea is to affect the profile drag of the wing and if it is possible to reduce also the induced drag. Until now, the profile drag of the wing is altered via active flow control, when mainly mitigation of the flow separation is needed (Kitsios et al. (2006)). However, in the present study, it is proved that alteration of the profile drag is very efficient even if the flow does not separate. In the context of this concept, a novel active control methodology is proposed, which increases the aerodynamic efficiency of the wing. Low velocity jets and large blowing slots proved to be the best configuration for saving energy.

2. Numerical set-up and description of the active flow control configuration

2.1. Numerical modeling

Both, natural and controlled flow are examined at Re=2.5 x 10^6 and at 5 angles of attack, namely at 4^o,6^o, 8^o, 10^o and 12^o. Travel speed is U_∞ =70 m/s, the chord's length is c=0.52m and the semi-span is b=1.7 m. Those values are derived from the detailed experimental study of McAlister and Takahashi (1991) for validation purposes. The examined wing has AR=6.6 and its' geometry is plotted in fig.1. The model is bounded by a parallelepiped with dimensions LxWxH= 15c x 7.5c m x 5c (fig. 2), where c is the chord's length. The blockage ratio is less than 1%.

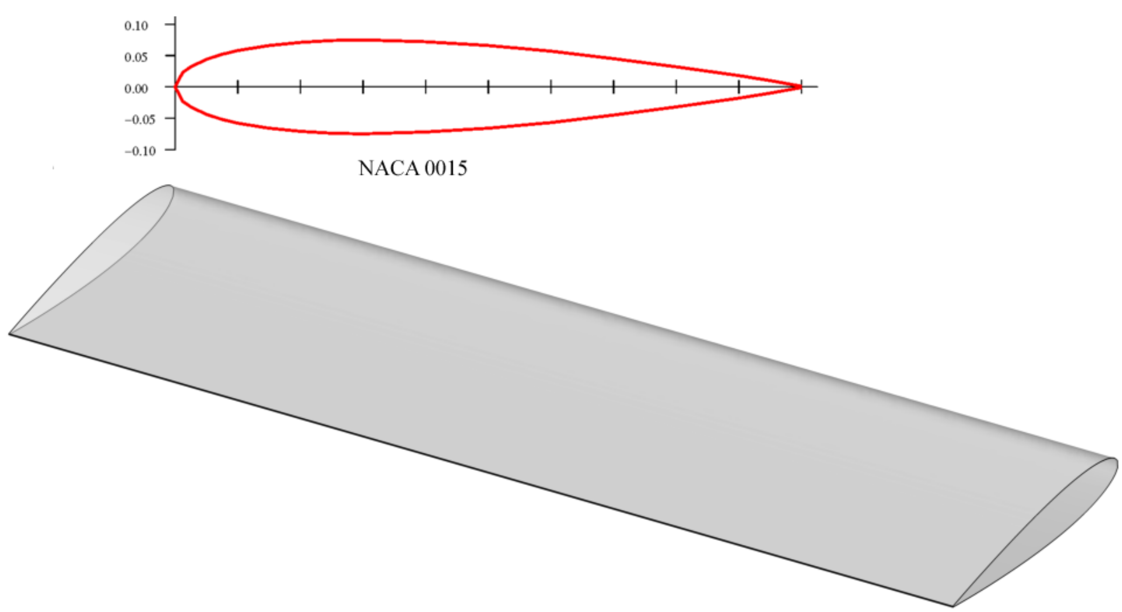

Fig. 1. Geometry of the wing and profile of the section.

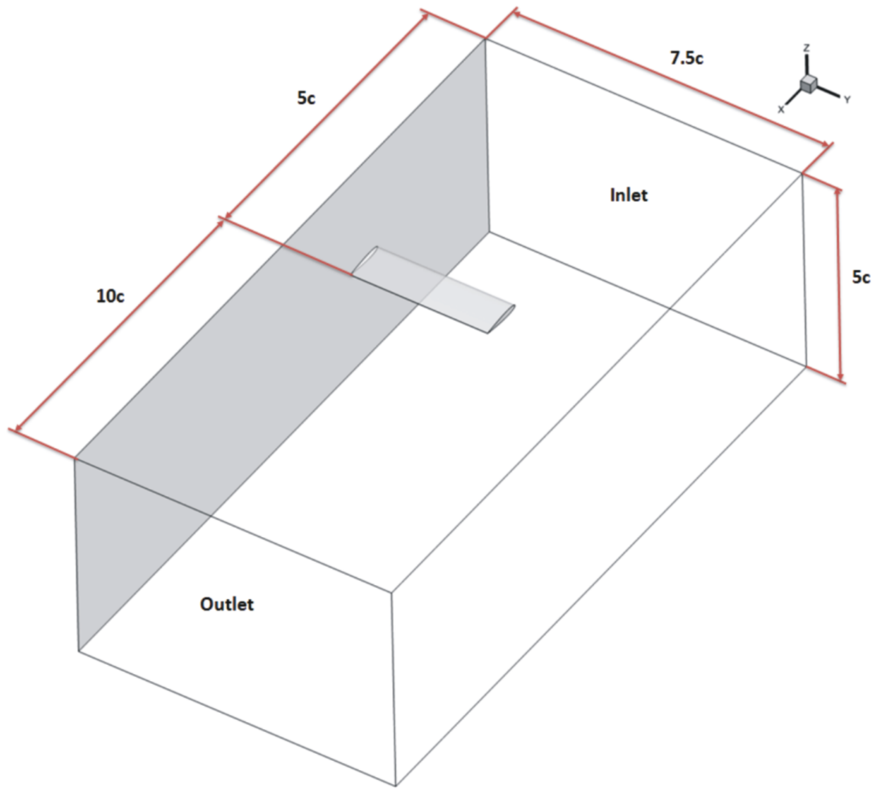

Fig. 2. Dimensions of the computational domain in chord lengths.

In the present study all the numerical simulations are performed in the framework of the commercial flow solver Ansys Fluent 13.0. The Navier-Stokes equations are integrated by the finite-volume method. The flow is considered to be fully turbulent, incompressible and steady-state. Turbulence is accounted for by a high Reynolds version of the Spalart-Allmaras model embedded in this solver (Spalart and Allmaras (1992)). All the terms of the equations have been discretized by a third-order MUSCL scheme based on Van Leer's (1979) research to reduce the numerical diffusion of the discretized equations through the log-law and the outer region. The boundary conditions used in those simulations are a constant velocity inflow profile with constant turbulent viscosity at the inlet of the domain , a zero stream-wise gradient outflow condition at the downstream area, no-slip condition for the wing and symmetry condition for the lateral and vertical boundaries.

The present modeling constitutes a compromise between accuracy and computational cost, since at such high Reynolds number flow the Unsteady Reynolds Averaged Navier Stokes (URANS) or Large Eddy simulations (LES) are very expensive or even prohibitive. However, it has to be remarked that the wing flows even at low angles of attack are substantially unsteady and transitional with strong vortex shedding. The steady-state approximation generally converges close to the time averaged results of the URANS simulations, but it has to be validated with relative experimental measurements. Spalart-Allmaras model is quite accurate for attached flows as in the present case, but the drag force is always over-predicted. The main source of this over-prediction is the deficiency of the model to predict the place and the nature of the transition process, which is determinant at low angles of attack. Nevertheless, as it will be shown in the present study, the model becomes more promising at higher angles of attack (8^o -12^o).

The Navier-Stokes equations are discretized and integrated on a hybrid mesh consisting of 2.2 million cells (fig. 3), which is generated by ICEM CFD 13.0 software. The grid is divided in two regions based on the cells topology and the nature of the flow: the first region consists of prismatic cells, which lie through the whole inner layer of the boundary layer (y+<100) and the second consists of tetrahedral cells, which are refined close to the last prismatic layer and gradually grow far away from the wing. The viscous length-scale values on the whole wing's surface is always y+<1.

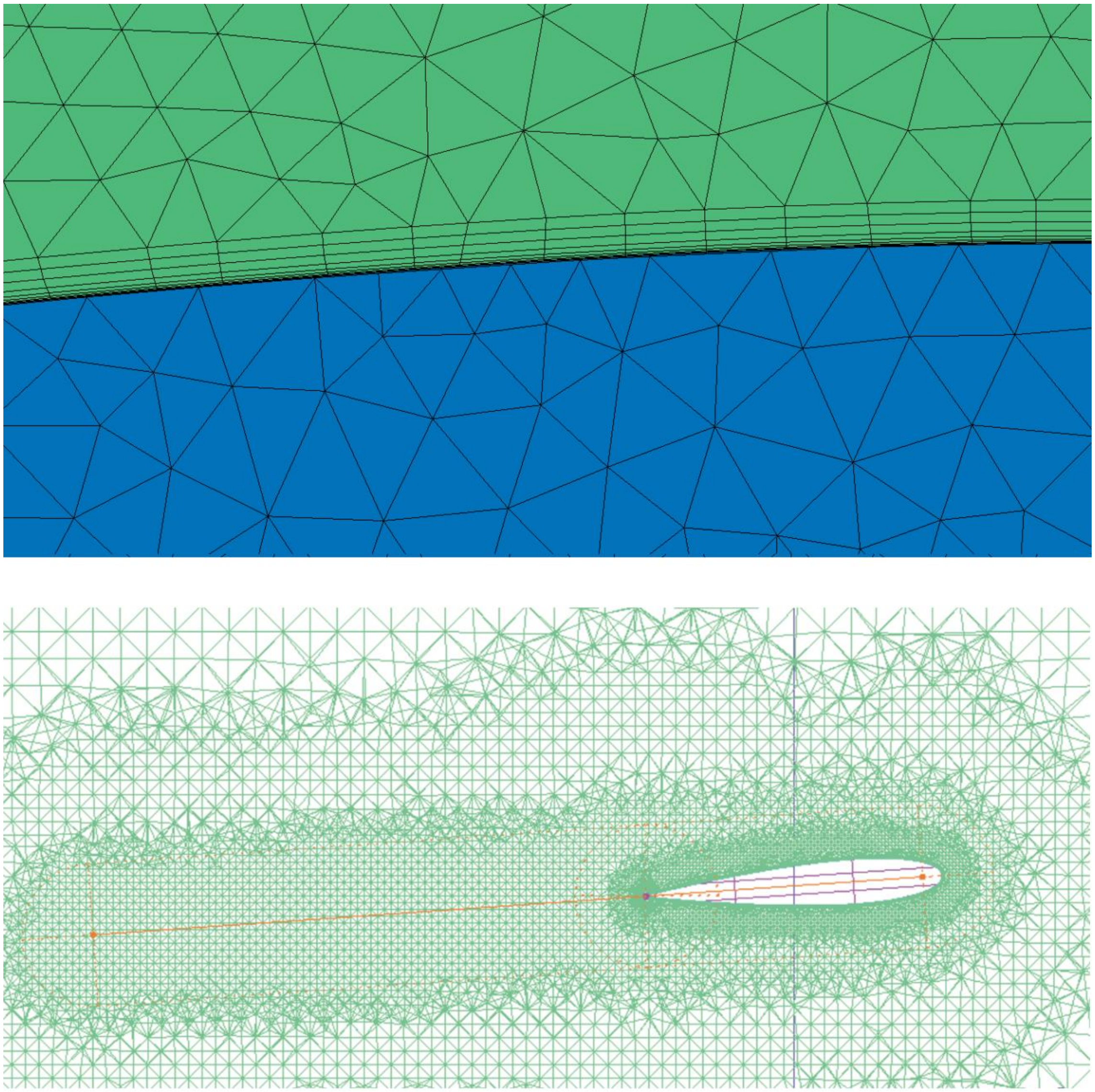

Fig. 3. Generated mesh in the vicinity of the wing (top) and farther (bottom).

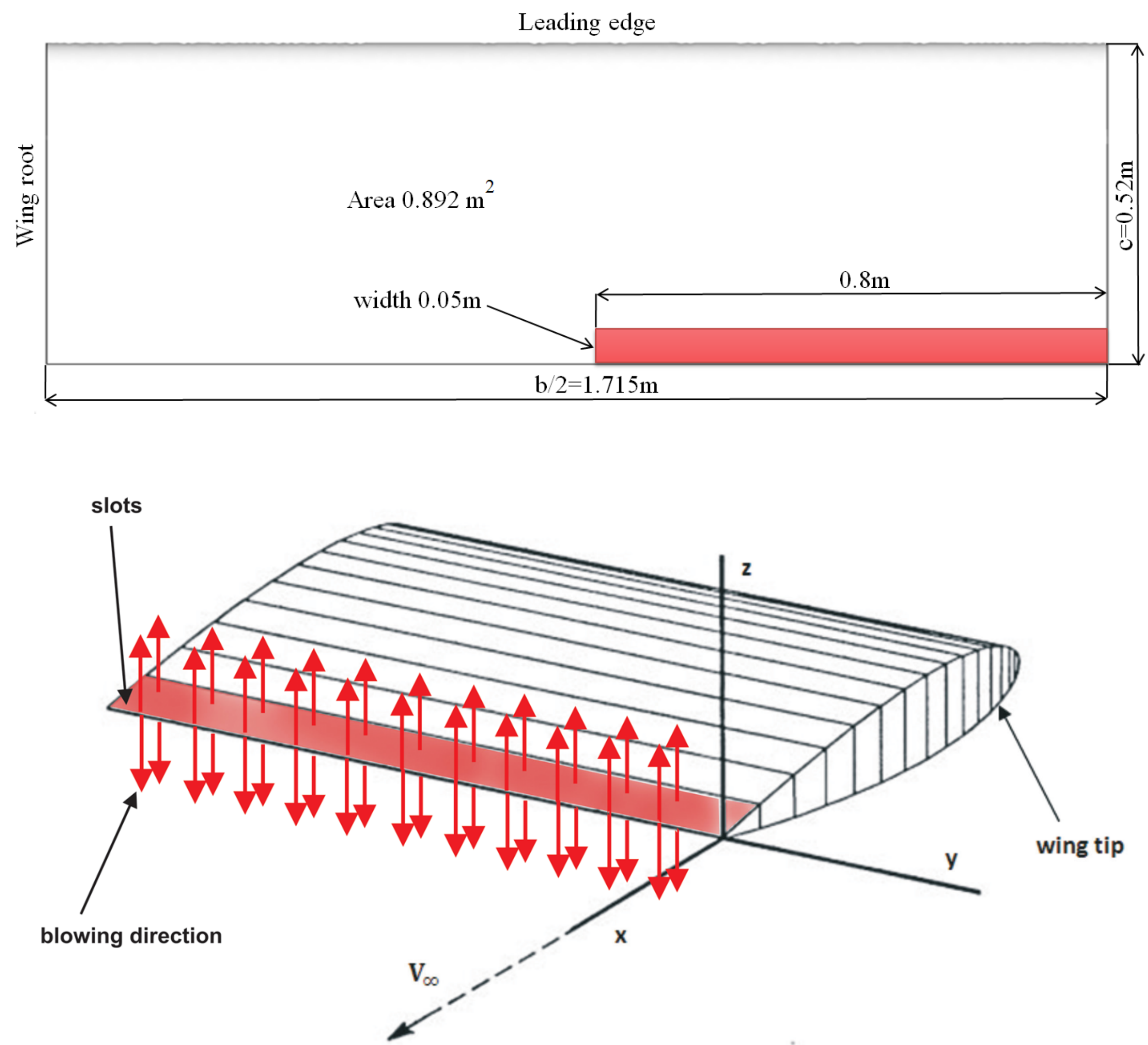

Fig. 4. Top view of the wing with the embedded blowing surface (top) and direction of blowing for the most successful case (bottom).

2.2. Description of the active flow control configuration

The final configuration consists of two large blowing surfaces. The upper one has area of 0.042 m^2 and the lower one 0.038 m^2. They are placed close to the trailing edge and they extend from the wingtip 0.8 m (half mid-span) towards the inboard part of the wing. The whole configuration from a top and close view is depicted in fig. 4. In the present study, the blowing velocity vector acts always in the vertical direction (normal to the free stream speed). The ejected flow from those blowing surfaces is assumed to have constant velocity and turbulent viscosity profile following the top hat velocity distribution (Geissler (2010)). Nevertheless, a lot of uncertainties arise by this assumption, which are usually not addressed in the majority of the research studies. In real applications, the flow in the vicinity of the slot is highly dependent upon the development of the flow inside the pipes of the actuation equipment. There is also dependence on the ratio between the jet velocity and the free-stream flow speed. It has been observed that this condition does not reflect the physics of the flow for small pipes and low velocity ratios, although in most of the cases it does not affect the loads computations (Karabelas and Popela (2011). In a relevant NASA Workshop compiled by Rumsey (2004), this consideration was verified for the case of pulsed jets. Indeed, DNS simulations diverge with the experimental profiles at the slot's location. Nevertheless, in the present case the blowing is massive and the effects could be crucial only close to the edges of the slot. Therefore, the top hat velocity boundary condition appears to be suitable for such configuration.

3. Results and discussion

3.1. Actuation parameters

Before proceeding to the discussion of the physics for both regimes of flow, some further description of the actuation set up should be considered. As already stated in the first section, the flow from the blowing surfaces is assumed to have a constant velocity and turbulent viscosity profile. In the present study four different blowing velocities are applied onto the upper surface. The global velocity ratio V_{global} is defined as the ratio between the blowing velocity of the upper surface to the free stream speed:

$$V_{global} = \frac{u_{bl-upper}}{U_{\infty}} \tag{1}$$

and it ranges from 0.04 up to 0.34. The momentum coefficient of the blowing device is defined as follows:

$$C_{\mu} = 2\frac{u_{bl}^2}{u_{\infty}^2}\frac{A_{bl}}{S} \tag{2}$$

where u_{bl} denotes the blowing velocity of the upper surface, u_{∞} the free-stream speed, A_{bl} the total actuation surface and S the reference area of the wing. The momentum coefficient for this configuration ranges from $C_{\mu} = 0.003$ up to $C_{\mu} = 0.02$ and based on the literature studies, those values lie in the common range of the blowing devices. It will be shown in the successive sections that the performance of the wing is significantly affected by the ratio between the blowing velocity onto the upper surface and the blowing velocity onto the bottom surface. This ratio will be referenced here as the local velocity ratio and it is formulated as follows:

$$V_{local} = \frac{u_{bl-upper}}{u_{bl-bottom}} \tag{3}$$

In the examined cases it ranges from 0.8 up to 1.25, which means that in some configurations the blowing is more intense on the upper surface and in some others it is more intense on the bottom one.

In all actuation configurations the energy efficiency is examined in order to assess the savings from every flow control case. It is widely known that blowing control demands high amounts of energy, which frequently exceed the saved energy by possible reduction of the drag force. In the present study, the energy efficiency ratio η is defined to evaluate the savings from every active flow control configuration. It is defined as the ratio of the net power which is saved from the active control divided by the total saved energy, thus the ratio of the net saved energy to the energy saved by drag reduction:

$$\eta = \frac{P_{drag\_reduction} - P_{blowing}}{P_{drag\_reduction}} = \frac{P_{net}}{P_{saved}} \tag{4}$$

3.2. Physics of the natural and controlled flow

The flow is controlled by two large slots, which are placed in the rear part of the wing and extend from the half length of the semi-span up to the wing tip area. Initially, the main purpose of this configuration was to reduce the total drag by altering the downwash distribution downstream of the wing. While this could be achieved by blowing only from the upper or the lower surface, the lift force could not be stabilized and in most of the times was lower than the computed force in the natural flow regime. However, when applying simultaneous blowing to the upper and lower

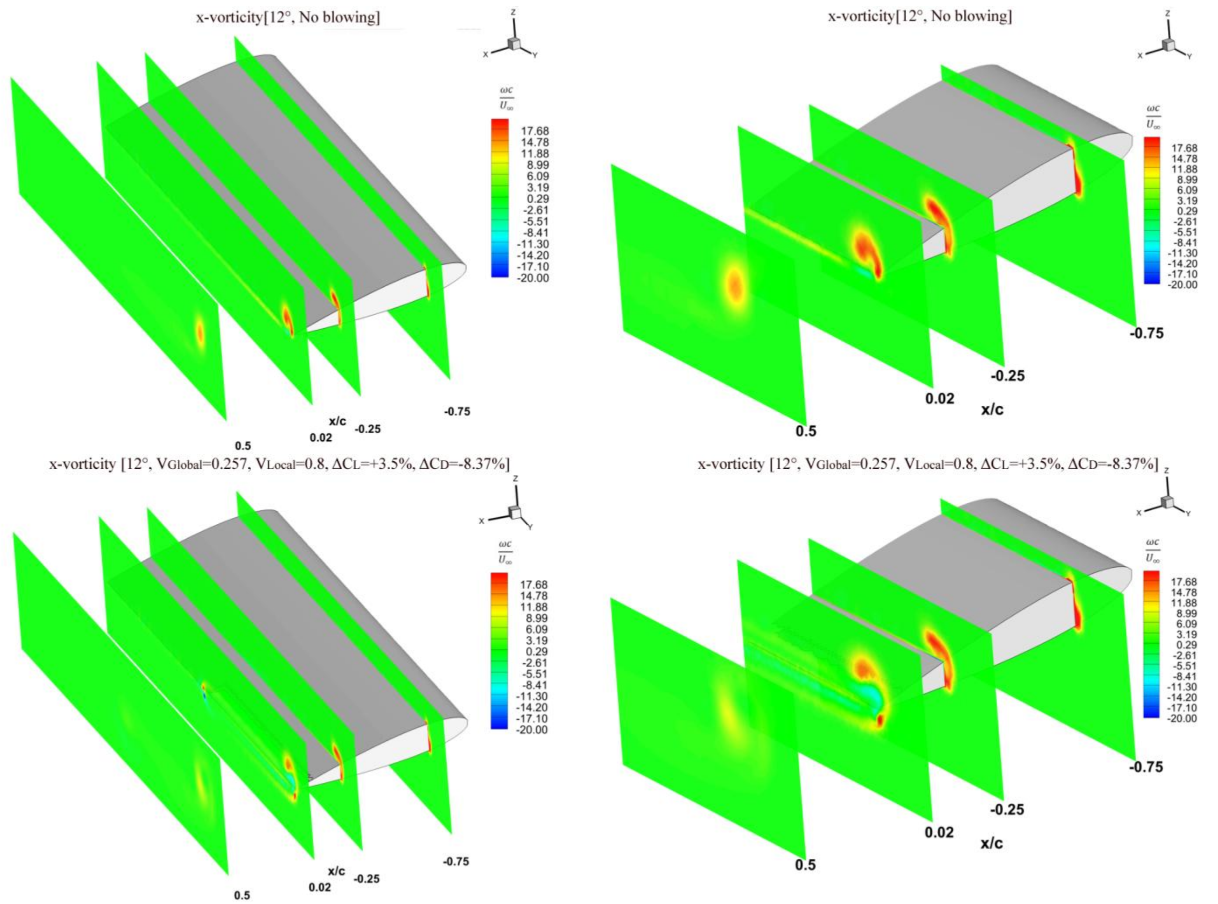

Fig. 5. Dimensionless axial vorticity distribution in the flow direction at a=12^o, for the natural (top) and a selected controlled flow case (bottom).

surfaces, the lift could remain the same or increased, while the drag is decreased.

The present active control affects globally and locally the flow-field. The dimensionless axial vorticity at a=12^o is plotted in fig. 5 for the natural and a selected blowing case. In the latter case the parameters are $V_{global} = 0.25$ and $V_{local} = 0.8$. The lift is 3.5% higher than the natural flow value and the drag is 8.37 % lower respectively. When no control is applied, the axial vorticity starts to emanate mainly from the lower surface and then starts to shift towards the wing tip area and the upper area of the wing. Eventually at the trailing edge area a well formed “double core” vortex is observed, where most of the vortical action is indicated slightly inwards (towards the root). Further downstream, both cores merge forming a single core vortex, which moves upwards and inwards and diffuses quite fast. The observed patterns are similar to those ones plotted for the low Reynolds number flow measurements of Margaris and Gursul (2010). However in both experiments the vortex diffusion was much weaker from the computed one. Farther from the trailing edge (*x/c*>2), based on a relevant experimental PIV study of Huppertz et al. (2005), vortex diffusion is increased. This is predicted here, but still the diffusion rate is overestimated. This result is mainly attributed to the numerical dissipation of the solver, which can't be avoided with the present resolution of the mesh. This is normal result in most of the RANS simulations studies, since the meshes are limited by the number of cells and can't be refined farther from the wing (Monsch (2007)). Blowing from both surfaces does not appear to alter the vorticity distribution upstream of the control. However, close to the trailing edge, the axial vorticity is considerably diffused forming a small layer of negative axial vorticity between the two main vortical structures. Those structures merge again to a single core vortex. The diffusion rate of the tip vortex is higher than in the natural flow. This reached conclusion, raise some ideas, whether such control could be also used for deploying faster decay of the aircraft wake vortices. Another two areas of high vorticity appear also close to the mid-span position, where blowing begins to apply. Those vortices with different sign of vorticity are expected to be formed, since the vertical blowing action from upper and lower surfaces, impose directly a significant amount of vorticity (positive to the upper and negative to the lower area) to the undisturbed three dimensional cross-flow.

Vertical velocity distribution is plotted in fig. 6. Blowing changes the entire flow development close to the trailing edge and downstream of the wing. In the wing tip area above the wing, the downwash is greatly weakened and the main contribution comes from the upper blowing surface. In the inward part of the wing, where blowing is not applied, the downwash follows the natural flow distribution. The positive vertical velocity values at $\frac{x}{c} = 0.5$ are quite lower compared to the respective ones in the natural flow regime. This conclusion is consistent with the previous vorticity plots. In fig. 7 the vertical velocity is plotted at three different sections of the wing's semi-span. At $\frac{y}{b} = 0.37$ where blowing is not applied, the flow fields are almost identical. At $\frac{y}{b} = 0.59$, blowing is applied and the effects are pronounced. The natural downwash is suppressed and acts only closer to the leading edge, since the upper blowing immerses mass flow vertically. The bottom jet flow is more diffused than the upper one. Downstream of the trailing edge the wake is affected mainly from the bottom blowing jet. Close to the tip area at $\frac{y}{b} = 0.94$, the controlled flow is completely different from the natural flow. Indeed, the well-formed downwash observed in the natural flow regime, is now separated to two areas of similar velocity magnitudes. Between those areas, the upper jet is immersed into the flow and collides to the already oppositely directed flow. The effects of the bottom jet are similar of those observed at $\frac{y}{b} = 0.59$.

Pressure distribution is plotted in fig. 8 at two selected angles of attack of 4^o and 12^o and for the natural flow case and an optimized actuating parameters set up (see table 1: case "lift maximized") . The effects of active flow control are more pronounced close to the blowing area. The pressure close to the slots position increases, because the outer-flow decelerates, while it approaches the immersed jet. Through the slot, the pressure decreases and the flow starts accelerating by gaining some momentum in the vertical direction. This distribution of pressure leads to significant drag reduction, since the increased pressure still acts onto the rear part of the airfoil. Lift force increases mainly at low local velocity ratio, where the jet beneath the wing is stronger and decelerates the flow more intensively producing higher static pressure distribution.

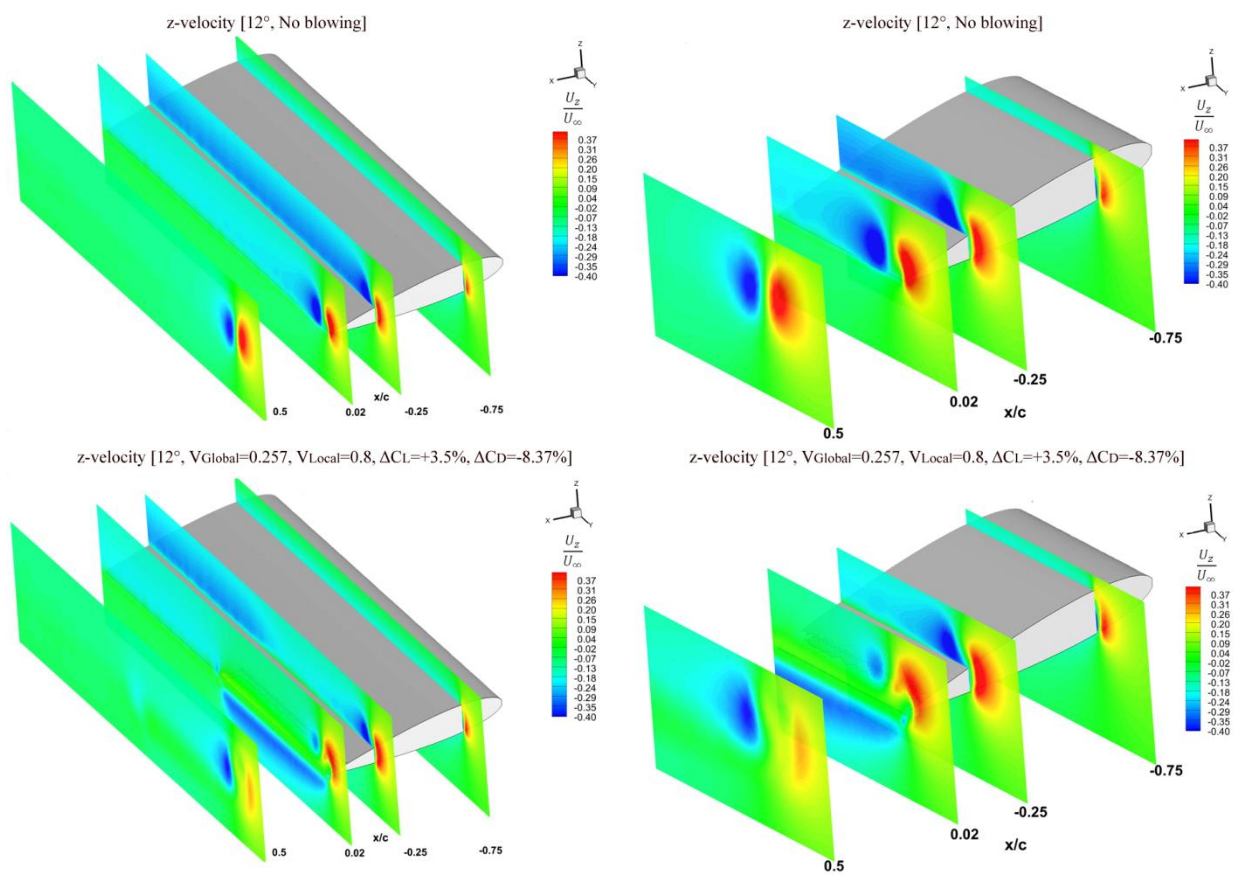

Fig. 6. Dimensionless vertical velocity distribution in the flow direction at a=12°, for the natural (top) and a selected controlled flow case (bottom).

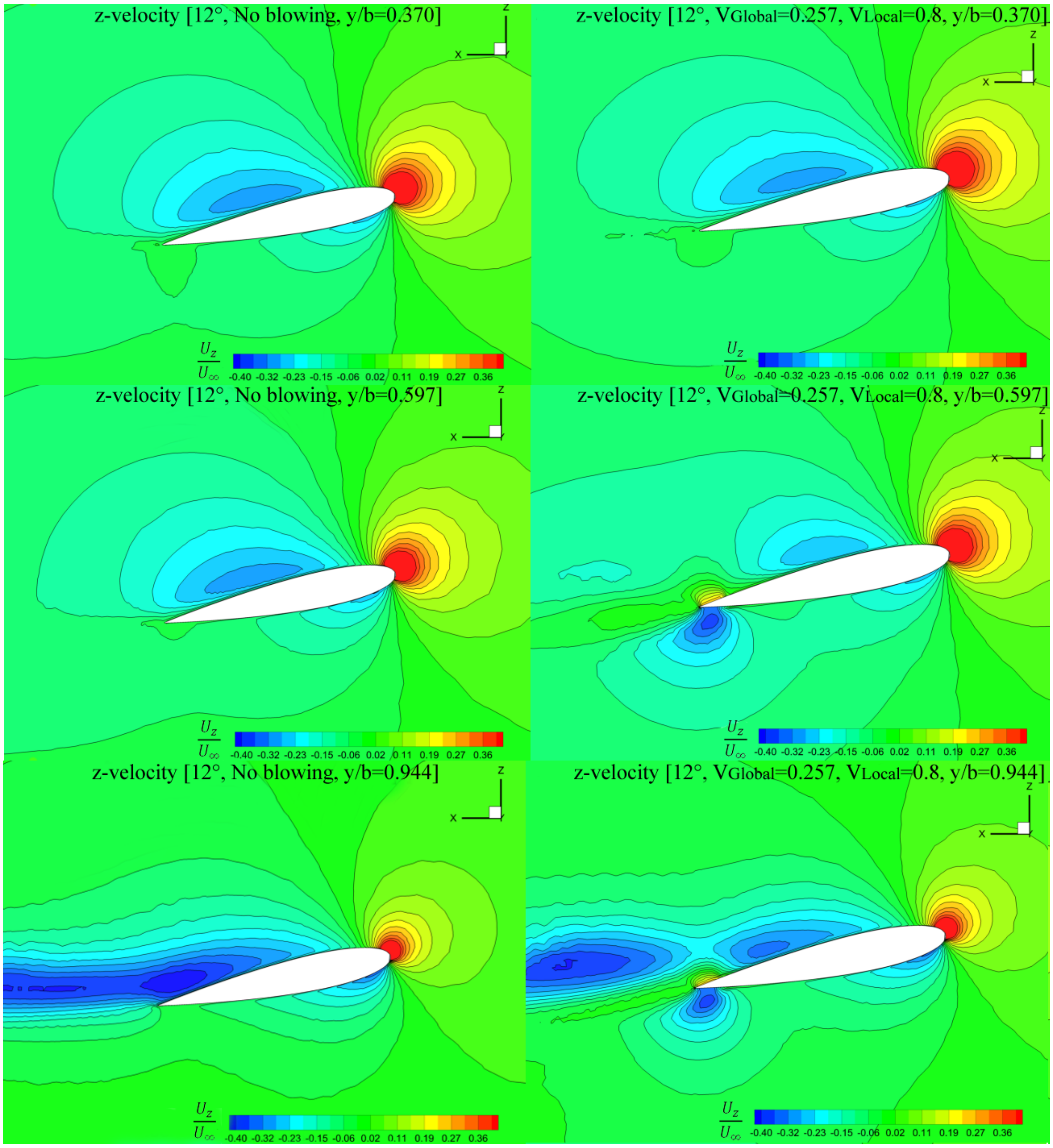

Fig. 7. Dimensionless vertical velocity distribution at different sections at a=12^{o}, for the natural (left) and a selected controlled flow case (right).

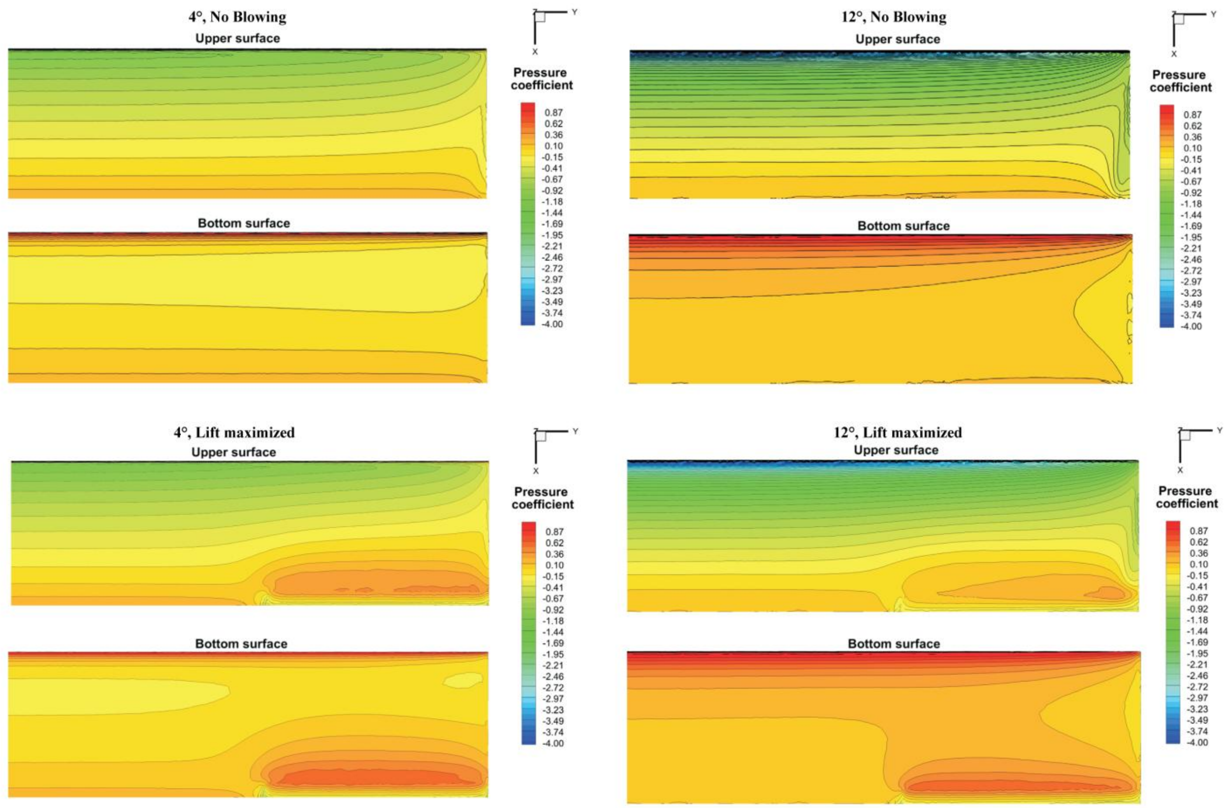

Fig. 8. Pressure distribution comparisons at a=4^{o} and a=12^{o} for the natural flow and the "lift maximized" case.

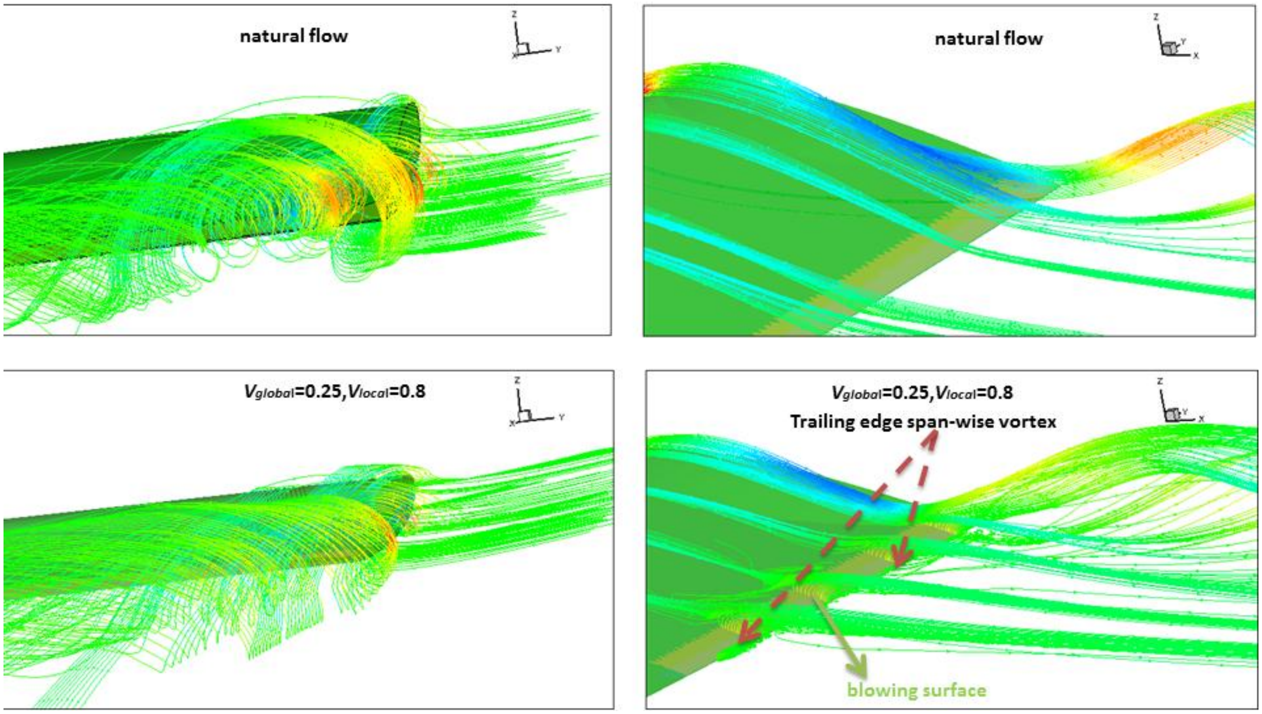

Fig. 9. Path-lines tracking for the natural flow and a controlled flow case. Trailing edge vortex is apparent in the controlled flow regime.

Qualitative results regarding the path-lines of the flow are plotted in fig. 9. The wing operates at a=12^o and the natural flow regime is compared to the case with $V_{global} = 0.25$ and $V_{local} = 0.8$. Volume path-lines colored by vertical velocity show clearly that in the controlled flow regime, the tip vortex is weakened and the flow possesses much lower vertical velocity but also rotational energy. In the inner region of the tip vortex, the natural flow rotates faster, thus possesses higher core vorticity. This conclusion is consistent with the direct comparisons of vorticity in fig. 5. When the path-lines are plotted at different span-wise sections of the wing, then it is possible to extract easily more information regarding the spatial development of the flow. When no control is applied, the flow remains attached to the surface and it moves inwards at the upper surface as expected. In the controlled flow regime, there are observed two distinct patterns. The flow forms a wavy structure (like overpassing a “step”) due to the superposition of the vertical jet velocity. A small but well-formed trailing edge vortex is also observed. This vortex extends through the whole span-wise length of the blowing surface. The wavy structure of the flow reveals that there is an exchange of momentum. Indeed, axial momentum is transformed to vertical momentum and the flow when approaches the immersed jet experiences a vertical shift. This flow development diffuses the wake vortex and reduce the vorticity close to the tip.

3.3. Aerodynamic loads and energy efficiency in controlled flow cases

The present actuating configuration is examined with the perspective to be capable of reducing the fuel consumption of modern aircraft structures and to be able in the future to control the aircraft at different regimes of flight. The computation of the total loads and the energy efficiency of such a device are the primary subjects of this study to ensure feasibility of both aforementioned targets. In the present configurations six local velocity ratios and 4 global ratios are examined. The wing operates at 5 angles of attack, namely 4^o, 6^o, 8^o, 10^o and 12^o and always at travel speed of 70 m/s. The results in the present study consider incompressible regime of flow, but the reported trends of the device could be also observed in compressible flow regimes.

Figure 10 plots the change in (%) of the force coefficients at $a=12^o$ as a function of the global velocity ratio at different local velocity ratios. The load curves at the other angles of attack follow similar distribution with greater absolute values in loads difference. It appears from this graph, that the device is not efficient in lift terms, when the local ratio is equal or greater than 1, namely when the upper blowing velocity is higher or equal to the bottom one. It could be efficient only at low global ratios. For instance at $V_{local} = 0.8$ and $V_{local} = 0.9$, lift increase is obtained at most of the examined global ratios and in most of the cases is combined with drag reduction. This performance is suitable for flight regimes, where increase in lift is needed, therefore in some accelerating climbing or landing cases. In cruise conditions, where stabilized lift accompanied with drag reduction is needed, then higher values of V_{local} should be imposed. However, via the proposed control, drag reduction is attained at almost all global velocity ratios. The aerodynamic efficiency of the blowing device is depended also upon the performance at different angles of attack.

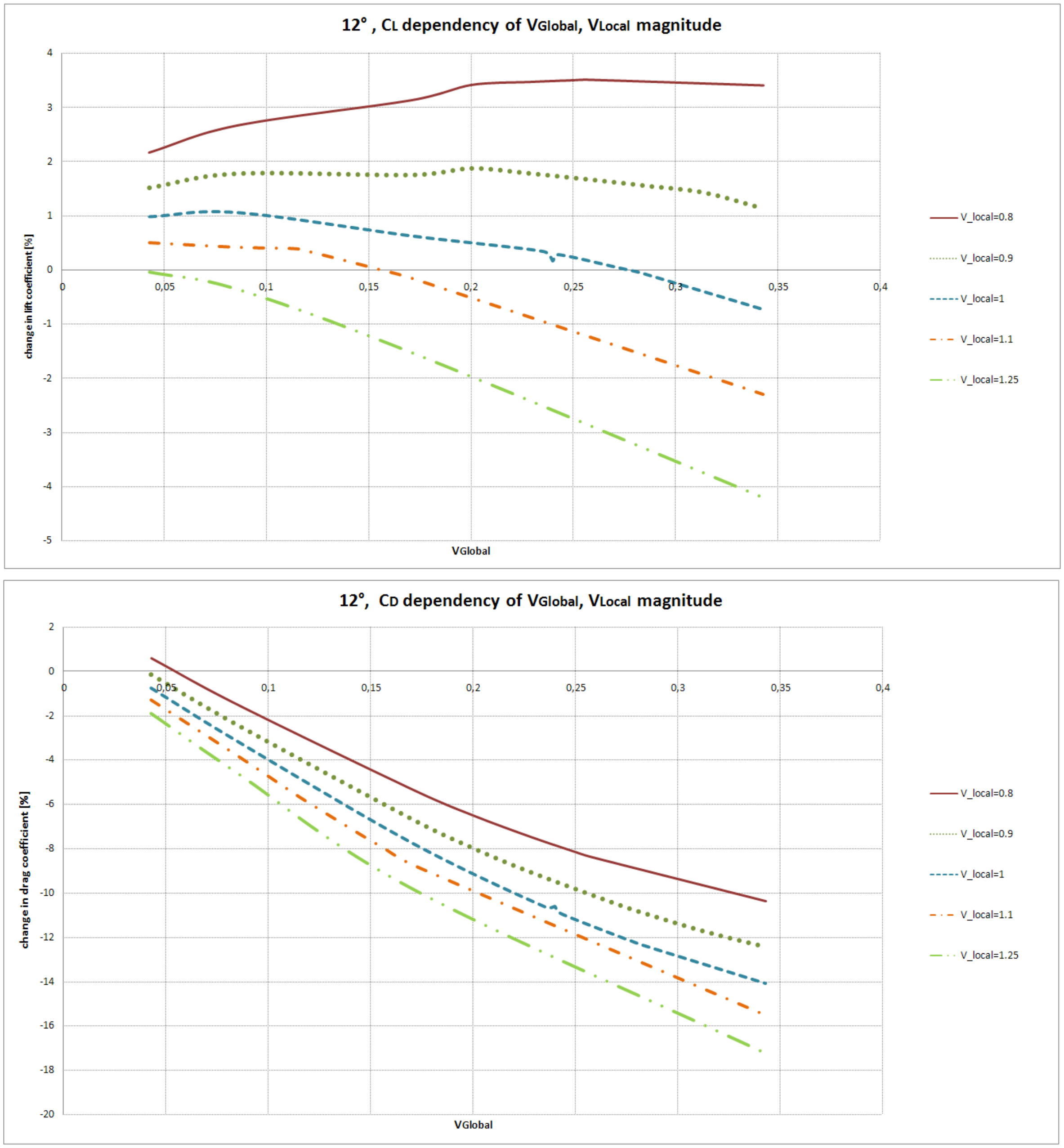

Fig.

Fig. 10. Variation of the lift (top) and drag (bottom) coefficients with V_{global} and V_{local} .

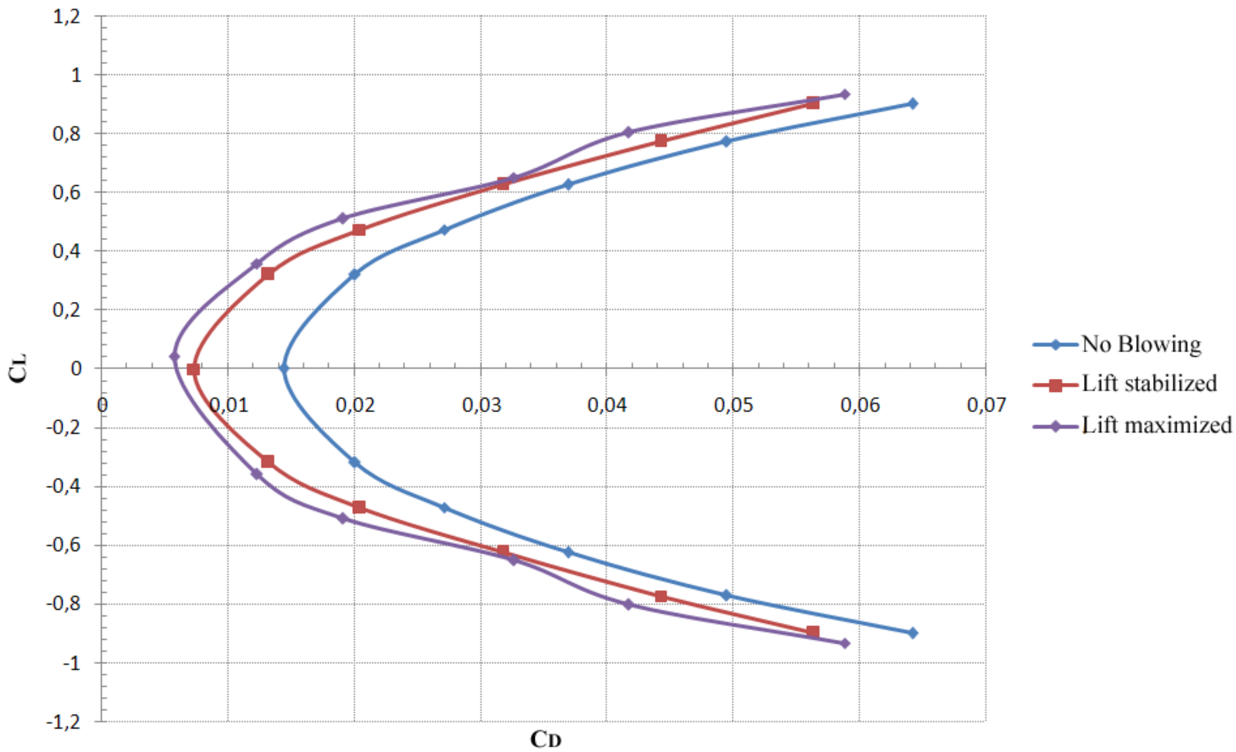

Fig. 11. Polar graph for the natural flow, the “lift stabilized” and the “lift maximized” cases.

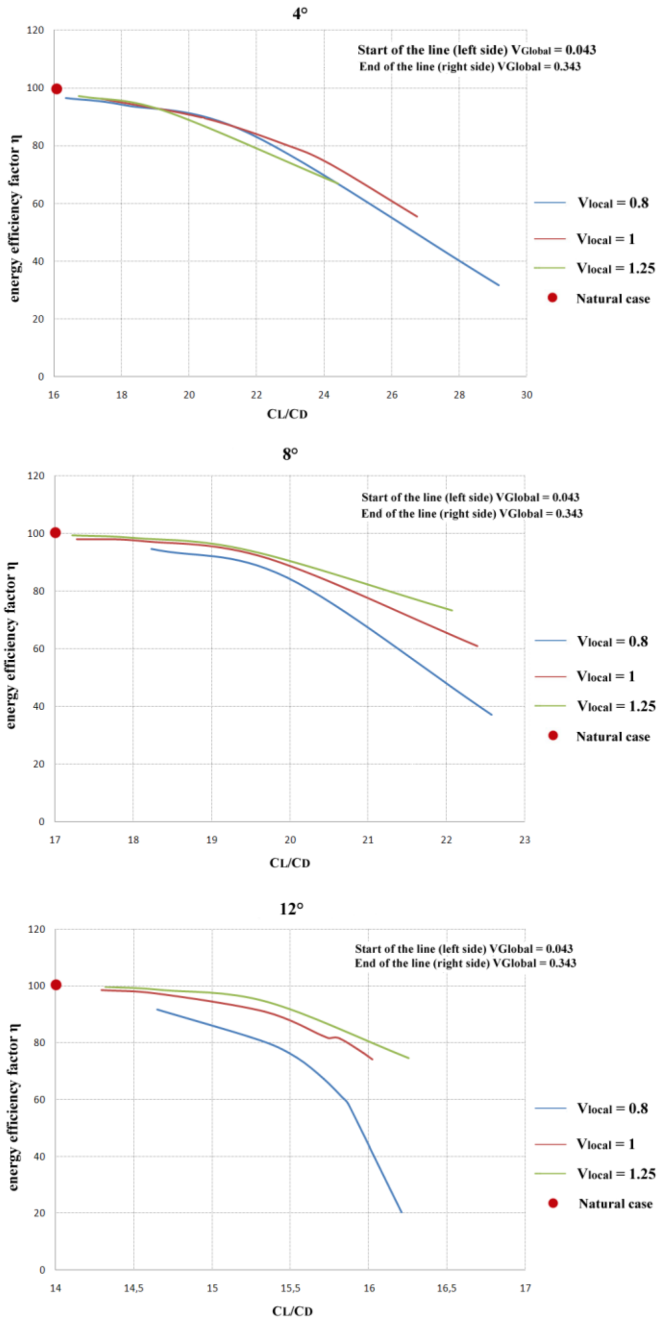

Fig. 12. Energy efficiency factor as a function of the glide ratio at different V_{local} values. Results at a=4^o (top), a=8^o (middle) and a=12^o (bottom).

Fig. 11 plots a polar graph for the natural flow and the two selected active flow control cases summarized in Table 1. It is revealed, that at every angle of attack, active control could be efficient in lift and drag terms and increase the ratio $\frac{C_l}{C_d}$.

Energy efficiency ratio is one of the main examined parameters in this study. The device for reasons of simplicity and uncertainty in the design of the actuation set-up, is considered as an ideal pump, where the demanding energy for blowing equals to the produced energy from the pump. Energy efficiency ratio at the vast majority of the examined cases is positive, which means that always the blowing energy was lower than the gained energy from the drag reduction. The most efficient solutions in energy terms are those with η close to 1. Fig. 12 plots the energy efficiency as a function of the ratio $\frac{C_l}{C_d}$ at different local ratios. Significant increase of the ratio is attained with still high values of η. It has to be highlighted, that in all computations of the energy efficiency factor, the gain in energy is based on the drag force reduction, as it is commonly considered. However, when the lift force increases an extra energy term is introduced to the balance of energy, which increases the value of η. Nevertheless the contribution of the lift force to the thrust of the wing is strongly depended upon the regime of flight. In future study, the aerodynamic results will be correlated to the flight operating conditions and the final gained energy income will be evaluated.

4. Conclusions

The main outcome from this research is that the implementation of active flow control with relatively large blowing surfaces and low jet velocity magnitudes, appears to be a viable solution for energy efficient and less polluting flights in aerospace applications. The testing of a single profile (NACA 0015), does not guarantee necessarily high levels of effectiveness in other cases. However, it is evident from this analysis, that there is space for obtaining energy efficient results by modifying the parameters of the actuation set-up, dependent each time upon the given profile. A side application of this concept and an interesting field of further research, could be the feasibility of controlling an aircraft without the main wing control surfaces, such as the ailerons, flaps and slats. Future research is directed towards the experimental verification of the concept, the testing of other wing geometries and the possibility of replacing the main control surfaces of the wing.

5. References

Coimbra, R.F.F., Catalano,F.M. The effect of wingtip blowing on the vortex drag. ICAS 2002 Congress, 2002.

Dunham, R.E. Unsuccessful concepts for aircraft wake vortex minimization NASA SP-409, 1976.

Abd.Y.Gandouz, Suliman. Study of vortex trap on low aspect ratio wing with NACA 0015 cross section. Masters thesis, Universiti Tun Hussein Onn Malaysia, 2011.

Geissler, W. A family of CFD boundary conditions to simulate separation control, Aerospace Science and Technology, Vol. 14, pp. 494-504, 2010.

Gerz,T. , Holzapfel, F., Darracq, D. Commercial aircraft wake vortices, Progress in Aerospace Sciences, Vol. 38, pp. 181-208, 2002.

Huppertz, G., Zurheide, F. , Schröder, W. Investigation of vortex-wake/engine-jet interaction in the near wake of a swept wing, Project Wakenet 2, Institute of Aerodynamics, RWTH Aachen

Karabelas, S. J. and Popela, R. Derivation of a surface boundary condition for continuous blowing. Industrial report No LU50-2011-VW.AD for Volkswagen company, 2012.

Katz, J. , Plotkin, A. Low-speed aerodynamics, McGraw-Hill Inc., 2001.

Kitsios, V. , Kotapati, R. B. , Mittal, R. Ooi, A. , Soria, A. and You, D. Numerical simulation of lift enhancement on a NACA 0015 airfoil using ZNMF jets, Center for Turbulence Research, Proceedings of the Summer Program 2006.

Lim, Hock-Bin: Numerical study of the trailing vortex of a wing with wing-tip blowing, Joint Institute for Aeronautics and Acoustics TR-112, 1994.

Margaris, P., Gursul, I. Vortex topology of wing tip blowing. Aerospace Science and Technology, Vol. 14, pp.143-160, 2010.

McAlister, K.W,Takahashi, R.K. NACA 0015 wing pressure and trailing vortex measurements

NASA report 3151, 1991.

Mineck, R.E. Study of potential aerodynamic benefits from span-wise blowing at

wingtip NASA technical paper 3515, 1995.

Monsch, S. C. A study of induced drag and span-wise lift distribution for three dimensional inviscid flow, Master Thesis, Clemson University, 2007.

Pope,S.B.: Turbulent Flows, Cambridge University Press, 1995.

Spalart, P.R. ,Allmaras, S.R. A one equation turbulence model for aerodynamic flows. Proceedings of the 30th AIAA Aerospace Sciences Meeting and Exhibit, Vol. 92, 1992.

Rumsey, C. L. Proceedings of the Workshop on CFD Validation of Synthetic Jets and Turbulent Separation Control, 2004.

Tavella,D.A., Roberts,L.: A theory for lateral wing-tip blowing Joint Institute for Aeronautics and Acoustics TR-60, 1985.

Van Leer, B. Towards the Ultimate Conservative Difference Scheme, V. A Second Order Sequel to Godunov's Method. J. Comput. Phys. Vol. 32, pp. 101–136, 1979.

Zimmer, H.: The Aerodynamic Optimization of Wings at Subsonic Speeds and the

Influence of Wingtip Design, NASA report TM-88534, 1987.

Yadlin,Y., Shmilovich,A.: Flow control of airplane trailing wakes, Boeing, 2008.

Zheng, Y. and B.R. Ramaprian, An experimental study of wing tip vortex in the near wake of a rectangular wing, Report No. M ME-TF-93-1, Washington State University,Department of Mechanical and Materials Engineering, 1993.